

## Article

# Spatio-Temporal Variation of Extreme Heat Events in Southeastern Europe

Krastina Malcheva <sup>\*</sup>, Lilia Bocheva  and Hristo Chervenkov 

National Institute of Meteorology and Hydrology, 1784 Sofia, Bulgaria; lilia.bocheva@meteo.bg (L.B.); hristo.tchervenkov@meteo.bg (H.C.)

\* Correspondence: krastina.malcheva@meteo.bg

**Abstract:** Many studies in the last few years have been dedicated to the increasing temperatures and extreme heat in Europe since the second half of the 20th century because of their adverse effects on ecosystems resilience, human health, and quality of life. The present research aims to analyze the spatio-temporal variations of extreme heat events in Southeastern Europe using daily temperature data from 70 selected meteorological stations and applying methodology developed initially for the quantitative assessment of hot weather in Bulgaria. We demonstrate the suitability of indicators based on maximum temperature thresholds to assess the intensity (i.e., magnitude and duration) and the tendency of extreme heat events in the period 1961–2020 both by individual stations and the Köppen’s climate zones. The capability of the used intensity-duration hot spell model to evaluate the severity of extreme heat events has also been studied and compared with the Excess Heat Factor severity index on a yearly basis. The study provides strong evidence of the suitability of the applied combined approach in the investigation of the spatio-temporal evolution of the hot weather phenomena over the considered domain.

**Keywords:** maximum temperature thresholds; extreme heat event; Excess Heat Factor; Southeastern Europe; Köppen’s climate zones



**Citation:** Malcheva, K.; Bocheva, L.; Chervenkov, H. Spatio-Temporal Variation of Extreme Heat Events in Southeastern Europe. *Atmosphere* **2022**, *13*, 1186. <https://doi.org/10.3390/atmos13081186>

Academic Editor: Paolo Stocchi

Received: 30 June 2022

Accepted: 23 July 2022

Published: 27 July 2022

**Publisher’s Note:** MDPI stays neutral with regard to jurisdictional claims in published maps and institutional affiliations.



**Copyright:** © 2022 by the authors. Licensee MDPI, Basel, Switzerland. This article is an open access article distributed under the terms and conditions of the Creative Commons Attribution (CC BY) license (<https://creativecommons.org/licenses/by/4.0/>).

## 1. Introduction

Recent reports by the Intergovernmental Panel on Climate Change (IPCC) and the World Meteorological Organization (WMO) confirm that the global temperature has continued to increase in the past decade and has already halved the distance to the upper limit of 2 °C, compared to the pre-industrial period, above which the risk of irreversible climate change increases rapidly [1–3]. Numerous studies suggest that rising temperatures and most extreme heat events in the recent decades would not have occurred without human-induced climate change (e.g., [4–8]). Although heatwaves represented around 2% of the weather- and climate-related disasters recorded worldwide from 1970 to 2019, they have been accountable for 8% of disasters’ caused deaths [9]. In addition to higher rates of thermal stress and mortality [10–12], high temperatures and prolonged hot weather are related to reductions in productivity [13,14], substantial agricultural losses [15,16], wildfires, damage to transport infrastructure, power failures, and sharp jumps in water and energy consumption [17–20].

Europe has experienced several intense heatwaves since the beginning of the 21st century [8,21–24], which have been associated with about 90% of deaths and 4% of economic losses from disasters after 1970 [9]. The severity of the heatwaves is expected to increase in the second half of the century due to the increasing magnitude and variability in summer temperatures [1,25]. The rise in extreme heat events under the intermediate and high GHG emissions scenarios could affect the countries of Mediterranean and Eastern Europe significantly, even by the middle of the century, where the heat-related mortality could increase by a factor of 1.8 and 2.6, respectively, compared to the 1971–2000 period [4]. Generally, the

region around the Mediterranean basin, including Southeastern Europe, appears to be one of the most vulnerable to climate change, with an increasing intensity of extreme weather and heat events [1,21,26,27] and a further increase in the previously observed summer heatwaves' frequencies and durations [28–30]. In southern Europe, prolonged hot weather periods are a typical summertime phenomenon due to the warmer climate and larger-scale atmospheric dynamics that favor the thermodynamic processes and land-atmosphere feedback [26,31]. According to the updated Köppen–Geiger classification [32], the European part of the Mediterranean region mostly belongs to the mid-latitude temperate climate zone, comprising not only Mediterranean climate types with a dry hot/warm summer (Csa/Csb) and large areas with no dry hot/warm summer (Cfa/Cfb), but also areas with humid or dry continental climates with hot/warm summer (Dfa/Dfb or Dsa/Dsb, respectively) in the north [33].

Despite the rise in extreme heat events worldwide, there is still no universal definition of them, but the common agreement is that they are prolonged periods unusually hotter than normal. All definitions consider at least one air-temperature characteristic (daily minimum, maximum or average) and require a certain number of consecutive days where a particular threshold is exceeded, and most of these thresholds revolve around the upper tail of temperature distributions [34]. Three heat event characteristics—magnitude, duration, and frequency—are generally accepted, but there is no consensus about the thresholds or the event's spatial and time extent. Definitions based on fixed-temperature thresholds are of essential importance in assessing many socio-economic and environmental impacts. Percentile-based thresholds, corresponding to the local climatology, facilitate a comparison of different climates and regions, but percentile-based analyses are deprived of the physical intuition of actual temperatures [31]. The development of monitoring and early-warning systems has further expanded the set of heat event definitions [22,35–38].

The anthropogenic influence on the climate, as well as the natural fluctuations of the Earth's climate system, are distinguished by substantial regional variations in the different time scales [1]. Therefore, it would be inappropriate to restrict the definitional diversity, as it reflects the various physical mechanisms proposed as the proximate and underlying drivers of heat events [31]. Even a small change in the definition could have a considerable impact on the results of climate analyses or risk assessments [39,40]. The heat event indices suitable for both public and research applications should be easily understood, useful as impact indicators, seamlessly interpretable by climate records, and predictable with reasonable accuracy [37].

The WMO Expert Team on Climate Change Detection and Indices (ETCCDI) has defined 27 internationally agreed indices of climate extremes, including heat-related extremes, to facilitate the regional climate change analyses ([http://etccdi.pacificclimate.org/list\\_27\\_indices.shtml](http://etccdi.pacificclimate.org/list_27_indices.shtml)) (accessed on 16 July 2022). Later, the WMO Expert Team on Sector-specific Climate Indices (ET-SCI) enlarged the list of indices designed for heat event analysis based on a new definition, accounting for excessive heat accumulation and short-term thermal acclimatization (<https://climpact-sci.org/indices/>) (accessed on 16 July 2022). The indices developed on health-based definitions receive increasing attention, especially for early-warning purposes in large cities [41,42]. Numerous gridded datasets of climate extremes indices at global or regional scales, with different spatial resolutions, are already freely accessible (e.g., [43–48]). The ETCCDI/ET-SCI indices are defined and computed on annual or monthly time scales, which can lead to ambiguous results or the impossibility of being used in some climate applications requiring different time steps. Moreover, the recently developed indices of extreme heat events are not yet included in the gridded datasets. The thermal comfort indices usually refer to an “average” healthy person, thus excluding large groups of people with different or impaired thermoregulation, who are most vulnerable to extreme heat [49].

The deathly heatwaves during the last two decades changed the focus of research on heat extremes from pure climatology to impact assessment and event attribution. After the exceptionally hot summer of 2007 in Southeastern Europe, heatwaves have been an

object of many regional studies that used different approaches and indicators. Founda and Giannakopoulos [50] placed summer 2007 in the climatology of the previous century and examined similarities with the Mediterranean summers of the future. Pecelj et al. [51] assessed the bioclimatic conditions in Serbia during the summer heatwave events defined by the daily thresholds of the Universal Thermal Climate Index (UTCI) and the maximum air temperature. Urban et al. [52] concluded that the cumulative Excess Heat Factor explains the magnitude of excess mortality during heatwaves in the Czech Republic better than other characteristics such as heatwave duration or daily mean temperature. Tolika [30] used the Excess Heat Factor (EHF) index to detect, identify, and describe heatwaves in Greece. Piticar et al. [53] found a substantial change in EHF-based indices and a statistically significant increase in the number, frequency, and duration of heatwaves in Romania. Using a city-specific heatwave hazard index, Morabito et al. [21] revealed a significant increase in heatwave hazards in the southeastern European capitals. Katavoutas and Founda [54] proposed a new indicator of urban heat stress intensity, with a focus on a vulnerable area of the eastern Mediterranean, defined as the difference between urban and non-urban thermal stress levels based on the UTCI and Humidex indices.

The present study further develops previous research [55,56] in the context of the suitability of developed criteria and indicators for the quantitative assessment of hot weather in Bulgaria for an overall climate analysis of heat events in Southeastern Europe. The ability of the proposed hot spell indicator to detect extreme heat events has also been studied and compared with the Excess Heat Factor (EHF) index.

## 2. Data Sources and Data Pre-Processing

We selected a domain over Southeastern Europe (SEE) with latitudinal and longitudinal boundaries of 35° N–50° N and 15° E–30° E, respectively (Figure 1, red-line frame). This area almost entirely falls into the Mediterranean region, defined by the Mediterranean Experts on Climate and Environmental Change (MedECC) [4], which includes parts of central and eastern European countries with a continental climate.

Daily maximum and minimum air temperature data from 70 selected meteorological stations, which covered the study area relatively evenly, were used to investigate the spatio-temporal variations of extreme heat events (EHEs) in the period 1961–2020. Data from 12 Bulgarian meteorological stations, included in our previous research [56], were provided by the National Institute of Meteorology and Hydrology (NIMH)—Figure 1, represented by grey triangles. Data from stations outside Bulgaria were downloaded from three freely accessible sources: the European Climate Assessment and Dataset (ECA&D) project [57], the U.S. National Climatic Data Center (NCDC) Global Historical Climatology Network daily dataset (GHCNd) [58], and the U.S. National Centers for Environmental Information (NCEI) Global Surface Summary of the Day (GSOD) dataset [59]. These sources are used in many applications requiring daily data (e.g., [60–62]). The providers of the first two datasets apply strict procedures to ensure high-quality data that consist of the detection of outliers, data consistency, and other checks on the main meteorological elements [63,64]. The quality control procedures in GSOD are more limited, but daily summaries are supplemented by useful attributive information about the processed input data (<https://www.ncei.noaa.gov/data/global-summary-of-the-day/doc/readme.txt>) (accessed on 16 July 2022). ECA&D implements a two-step testing procedure for evaluating time series homogeneity [63]. GHCNd and GSOD do not support this type of information about time series homogeneity.

ECA&D is the primary source of observational data for the European region, but the number of stations in Southeastern Europe with freely accessible data and complete time series by 2020 is limited. Therefore, the GHCNd and GSOD datasets were used to complete a sufficiently dense set of stations for presenting the EHEs climatology.

The structure of the GHCNd dataset includes a source attribute, which indicates that hourly and daily data from different sources such as the Global Climate Observing System (GCOS), ECA&D and Global Summary of the Day (NCDC DSI-9618) are merged in the

time series available for the SEE domain. The latter source's daily maximum and minimum temperatures are included in GHCNd, only when provided as a nominal 24 h climatological summary as indicated in the SYNOP messages [64].

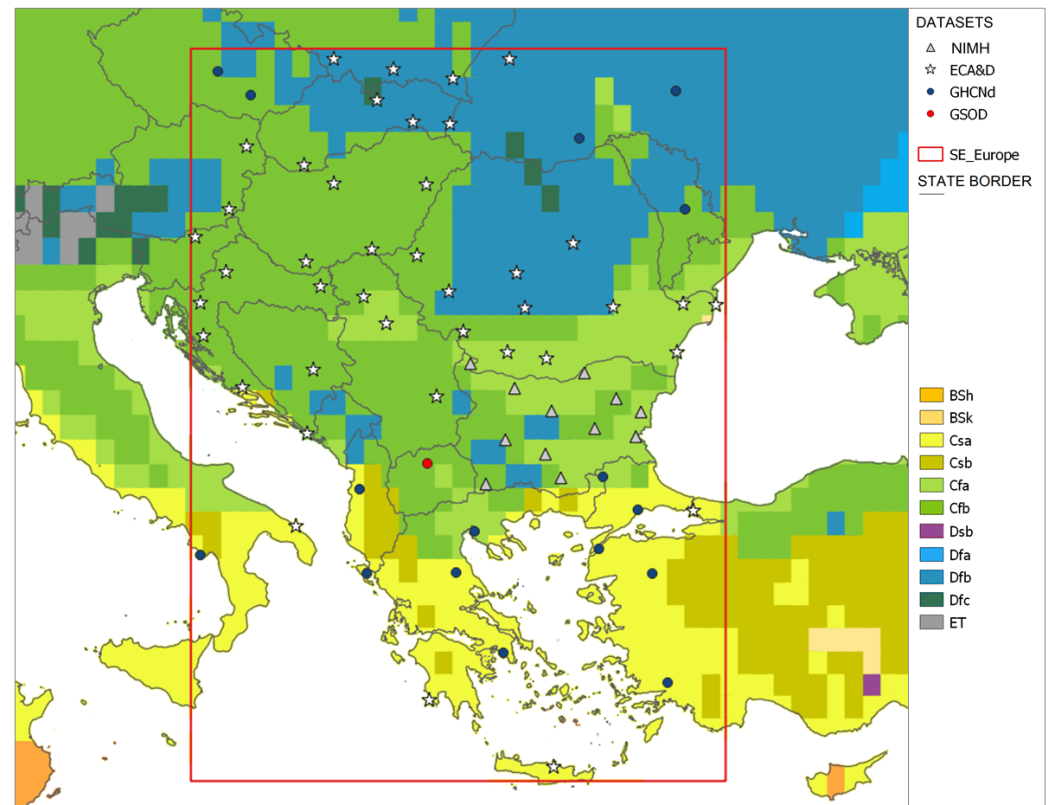


**Figure 1.** Location of meteorological stations used in the study on the background of the map of Köppen–Geiger classification (1951–2000) [32], data source: <http://koepfen-geiger.vu-wien.ac.at/present.htm> (accessed on 16 July 2022); the selected stations are marked as follow: grey triangles—12 stations from the NIMH network; blue and red dots—16 stations from GHCNd and one from GSOD datasets, respectively; asterisks—41 stations from ECA&D database.

GSOD data have been available generally since 1929, but the time series are sufficiently filled from 1973 to the present. In addition, when readings of the maximum or minimum thermometer are missing, the daily maximum/minimum temperature in GSOD is determined by the dry-bulb temperature from synoptic reports. If we separate the data by forming new samples of measured maximum/minimum temperatures (GSOD-m) and substituted maximum/minimum temperatures (GSOD-s), the comparison by stations indicates that the GSOD-s maximum temperatures are cooler while the minimum temperatures are warmer than GSOD-m (Appendix A, Figure A1). Due to these biases, we excluded all minimum/maximum temperatures obtained from incomplete 24 h observations. Moreover, we restricted the use of GSOD data mainly to auxiliary time series due to the large data gaps before 1973.

The selection of stations was organized as follows. Firstly, we explored the data sources looking for stations with available maximum and minimum temperature data since 1961 that fall into the defined above SEE domain. Next, we selected stations with no more than 20% of their data missing in the whole observational period and altitudes below 800 m, thus focusing the study's scope on the non-mountainous areas. Then, we reduced the number of stations with overlapping observational periods to one within a radius of 50 km to preserve a sufficiently high density of stations. The exclusion criteria accepted were the availability of data by 2020 and the homogeneity of the time series.

We selected 17 stations from the ECA&D blended dataset with homogeneous time series and 24 more stations for additional testing, assuming that inhomogeneities could be triggered by local or regional climate variations [63].

Generally, the merging of time series was avoided in our study except for Istanbul and Tirana stations when long enough, partially overlapping observational periods, available in the used data sources, were adjusted by simple linear scaling. The only case of extrapolation of time series over a large historical period (from 1961 to 1973), in order to preserve the relatively evenly spread of stations in the domain, concerned the Skopje International Airport station accessible by the GSOD dataset. Data reconstruction was made under the missing values imputation process before calculating the EHEs indices, using the R-package ‘missMDA’ [65]. For most stations in the southern part of the domain, the “no more than 20% missing data” selection criterion was not met, and several time series with 21–37% of their values missing, especially for minimum temperature, were used because of the above-mentioned reason.

The missing values were filled in by an iterative principal component analysis (PCA) imputation technique, which takes into account both the internal structure of data and the links between time series (Appendix B). The PCA-based spatio-temporal reconstruction of time series in data-sparse periods using periods with good data coverage and regionalization of time series with similar climatological characteristics is successfully applied by Tveito et al. [66]. In our study, the Köppen–Geiger climate classification and correlation between station data were used as regionalization criteria. The enhanced global dataset for the land component of the fifth generation of the European Centre for Medium-Range Weather Forecasts (ECMWF) atmospheric reanalysis ERA5-Land [67] was used as a reference dataset to improve the quality of the infilling of time series with medium to large data gaps.

ERA5-Land shows higher skill than other reanalysis products across geographically-diverse regions, which suggests that not only improvement in data assimilation but higher spatial resolution is critical to accurately reproducing extreme events observed from surface weather stations [68]. Although reanalyses contain some uncertainties, they are effectively used in gaps-filling procedures, even on sub-daily timescales [69]. The 2 m air temperature raw data from ERA5-Land were pre-processed in order to obtain daily maximum and minimum temperatures, as described in [70]. Since the ERA5-Land data are stored in netCDF files, all netCDF operations were performed by means of the software ‘climate data operators (CDO)’ [71].

Four homogeneity tests included in the R-package ‘trend’, Bartels test (a rank version of von Neumann’s ratio test), a Standard Normal Homogeneity Test (SNHT), a Buishand U-test, and Pettitt’s test [72], were applied to the time series of annual maximum and minimum temperatures from the reconstructed time series and abovementioned stations with problematic or missing homogeneity testing. The accepted rejection criterion was three or four failed tests at a 1% significance level.

Finally, in addition to the 12 stations from the NIMH network, 41 stations from the ECA&D database (Figure 1, asterisks), 16 stations from GHCNd, and one from GSOD (Figure 1, blue and red dots) were chosen to obtain a good enough coverage of the study area. The average distance between neighbour stations is 118 km. Most stations are located below 500 m a.s.l. Moreover, 17% of stations are located at airports, and 24%—are in urban areas (Appendix A, Table A1). The stations included in the study fall into three main groups of the Köppen–Geiger climate classification [32]—59% are characterized by temperate climates without a dry season (Cfa and Cfb), 21% have Mediterranean climates (Csa), and 20% of the stations have continental climates (Dfb).

### 3. Methodology

The shortcomings of threshold-based indices are well-known, but they are often more suitable when assessing the immediate impacts of temperature extremes on ecosystem resilience, human health, and quality of life. Depending on the research scope and aims,

temperature thresholds can reflect either biophysical constraints or local conditions derived from local climatology. The latter ones are generally inappropriate for larger-scale analyses. Using a definition of EHEs that only identifies extremely hot days may underestimate the risks associated with extreme heat, and inversely a less stringent threshold may overestimate the risks [73]. Although the risk assessment of extreme heat was not among the aims of the study presented in [55], the proposed approach may be helpful in sector-specific climate assessments. The main idea was to improve the methodology of hot spell analysis in order to reveal EHEs' climatic features in the non-mountainous part of Bulgaria, given its climatic diversity. Later, we propose three hot weather indicators and demonstrate their applicability based on data from 115 NIMH stations and the E-OBS dataset [56]. The present study aims to test the suitability of the developed indicators for an overall analysis of hot weather and EHEs in Southeastern Europe, bearing in mind that the share of Köppen's subtypes (Cfa and Cfb) prevailing in Bulgaria is almost 50% in the whole domain. The ability of the proposed hot spell indicator to detect extreme heat events has also been studied and compared with already proven climate indices, such as EHF.

### 3.1. Climatologically Justified Threshold Indicators for Bulgaria

The threshold indicators proposed in [56] were developed on daily maximum air temperature data ( $tx$ ) from 36 meteorological stations representative of the non-mountainous regions in Bulgaria using statistical modeling (Appendix C). In accordance with the obtained estimates, three climate indicators of hot weather were defined, as shown below.

1. The annual number of hot days ( $nhd32$ )—i.e., the annual count of days when  $tx > 32$  °C.
2. The maximum number of consecutive hot days ( $chd32$ )—i.e., the longest continuous calendar period when  $tx > 32$  °C.
3. The hot spell duration at different thresholds ( $hsd32/34/36/38/40$ )—i.e., the annual count of days when  $tx \geq 32, 34, 36, 38,$  and  $40$  °C for at least 6, 5, 4, 3, and 2 consecutive days, respectively.

The first indicator represents a general measure of unfavorable daytime thermal conditions; its long-term increase is related to the increasing frequency of prolonged hot spells. The second indicator delineates the upper bound of hot weather persistence. Finally, the third indicator allows a combined (intensity-duration) evaluation of EHEs in five categories. Although the  $hsd$  indicator is defined on a yearly basis, the technology of calculations allows the separation of events and their analysis. Thus, each category can be described by the EHE's intensity (*low/moderate/elevated/high/extreme*) and corresponding metric ( $hsd32/34/36/38/40$ ).

The significance and magnitude of trends in the threshold indicators were assessed through the non-parametric Mann–Kendall's test and Sen's Slope Estimator (see refs. [74,75] for details) using the R-package 'trend'.

### 3.2. Excess Heat Factor (EHF)

As an operative heatwave index, the EHF was first used in Australia. The EHF definition was proposed in 2009 as an improvement of the previous absolute or relative heatwave indices on a national level. The EHF measures the heatwave intensity at each location with an additional component to account for adaptation (Appendix D). Later, the EHF was utilized to examine the frequency, intensity, and duration of heatwaves on a global scale [34,36]. Moreover, the EHF provides public health stakeholders with a simple but efficient method to estimate excess heat exposure levels compared to other extreme-heat metrics or bio-climatic indices (e.g., [52,76]). The EHF's severity ( $EHF_{sev}$ ) metric permits the comparison of heatwave events and their impacts across the world and can be readily implemented within heatwave early warning systems [37,76]. For a given day  $i$ , the EHF severity ( $EHF_{sevi}$ ) is defined as follow:

$$EHF_{sevi} = \begin{cases} EHF_i / EHF_{p85}, & \text{if } EHF_i > 0 \text{ and} \\ 0, & \text{if } EHF_i \leq 0, \end{cases} \quad (1)$$

where  $EHF_{p85}$  denotes the 85th percentile of all positive EHF values calculated for a 30-year historical period.

Nairn et al. [37] defined three levels of EHEs severity as:

- L1 (low intensity): when  $0 < EHF_{sev} < 1$ ;
- L2 (severe): when  $1 \leq EHF_{sev} < 3$ ;
- L3 (extreme): when  $EHF_{sev} \geq 3$ .

The annual summaries of  $EHF_{sev}$  characteristics, such as mean and maximum magnitude, were calculated for the SEE domain based on daily maximum and minimum temperatures from complete time series. The results are presented via the zones of the Köppen–Geiger climate classification.

### 3.3. Software Products Used in the Research

All calculations completed on observational data were made in the free software environment R, version 3.6.2 [77], and RStudio 1.2 [78]. The maps shown in figures were prepared using QGIS 3.4.9-Madeira [79].

## 4. Results and Discussion

Many studies in the last few years have been dedicated to the increasing temperatures in Europe since the second half of the 20th century. As stated in [80], the increase rate is almost twice as rapid from 1985 to 2020 as in the whole period after 1951 (0.027 and 0.051 °C/year, respectively). The warming intensities depend on the season, with the largest summer warming of around 0.060 °C/year recorded in Central and Southern Europe. These findings are consistent with our results about trends in annual mean temperatures in the considered SEE domain obtained from the complete data series for the periods 1961–2020 and 1985–2020 (0.032 and 0.055 °C/year, respectively). As far as the focus of this research is on applying threshold indicators for EHEs analysis in a climatically diverse region, such as SEE, we additionally explored the maximum temperature features through zones of the Köppen–Geiger climate classification. The box plots in Figure 2 present the distribution of the calculated upper percentiles of the daily maximum temperatures at stations in the four climate zones. One can see that only the higher percentiles, usually used in EHEs definitions, fall into the range of the above-stated  $tx$ -thresholds.

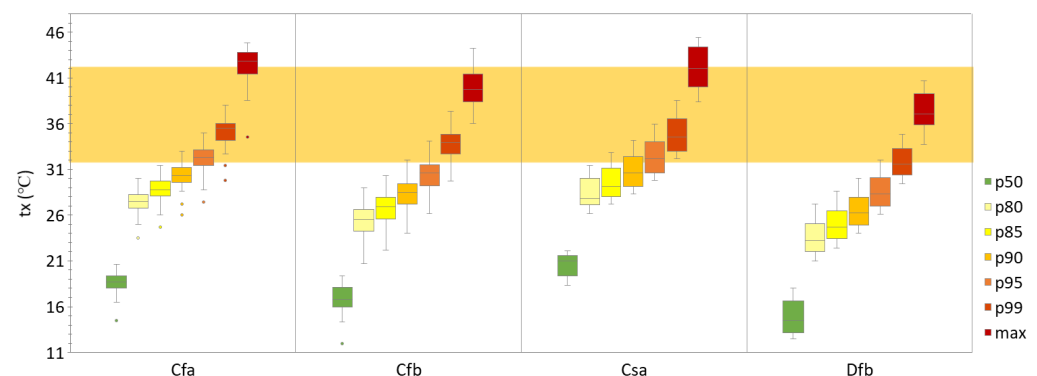


**Figure 2.** Medians (p50); 80th, 85th, 90th, 95th, and 99th percentiles (p80, p85, p90, p95, and p99) and absolute maxima (max) of daily maximum temperature  $tx$  time series for the period 1961–2020 by climate zones; the range of values used in threshold indicators is shown in light orange.

Table 1 shows the magnitudes of the trends in annual mean ( $T_a$ ), annual mean maximum ( $T_{mx}$ ), and annual maximum ( $T_x$ ) temperatures in the period 1961–2020 by climate zones. The largest average magnitudes are obtained for Cfb, followed by the Dfb, Cfa, and Csa climate zones.

Most stations with maximum trend magnitudes are located in the central part of the SEE domain, including one station (S10) in the hottest region of Bulgaria along the Struma

River valley. Unlike  $T_a$  and  $T_{mx}$ , which have statistically significant trends for all stations, the percentage of stations with a significant  $T_x$  trend varies between 40% (Csa) and 92% (Cfb). We demonstrated in [56] the suitability of estimated  $tx$ -thresholds (32, 34, 36, 38, and 40 °C) and corresponding duration thresholds (6, 5, 4, 3, and 2 consecutive days) to classify EHEs in the period 1961–2019. Consequently, our expectation is to obtain an accurate enough picture of EHEs that changes both by individual stations and climate zones in the SEE domain by applying the threshold indicators.

Figure 3 illustrates the long-term variation of the averaged-by-climate-zone indicators  $nhd32$  and  $chd32$  (calculated separately for each station), which reveals a clear upward, although not monotonic, tendency.

**Table 1.** Average/maximum values of Sen’s slope estimates (unit: °C/10 years) of statistically significant linear trends ( $p < 0.05$ , Mann–Kendall method) of the  $T_a$ ,  $T_{mx}$ , and  $T_x$  temperatures in the period 1961–2020 by zones of the Köppen–Geiger climate classification; stations’ IDs are shown in brackets (see Appendix A, Table A1), in which maximum values are reached; percentage of stations with statistically significant trends is also shown.

	Cfa	Cfb	Csa	Dfb
$T_a$	+0.29/+0.43 (S1) 100%	+0.39/+0.55 (S18) 100%	+0.24/+0.37 (S45) 100%	+0.34/+0.44 (S60) 100%
$T_{mx}$	+0.36/+0.50 (S10) 100%	+0.43/+0.63 (S21) 100%	+0.27/+0.43 (S56) 100%	+0.38/+0.50 (S66) 100%
$T_x$	+0.41/+0.66 (S10) 70%	+0.49/+0.74 (S28) 92%	+0.38/+0.63 (S48) 40%	+0.45/+0.70 (S60) 86%

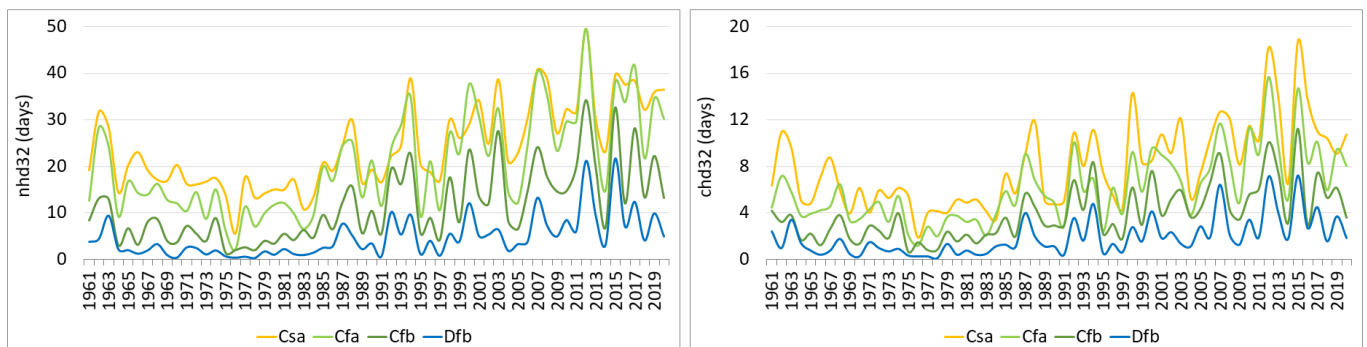


**Figure 3.** Long-term variations of  $nhd32$  (left) and  $chd32$  (right) indicators averaged by Köppen–Geiger climate classification zones.

Both indicators show statistically significant positive trends in most stations and a stronger worsening of daytime thermal conditions in the areas with hot summers (Table 2).

The average magnitudes of the  $nhd32$  trends ranged between +1.0 and +3.8 days/10 years (in Dfb and Cfa, respectively), and the maximum magnitude of +8.0 days/10 years was reached in the Csa climate zone. The  $nhd32$  maxima by stations vary between 4 and 97 days, with lower values occurring in coastal and northern stations. Almost all maxima were recorded between 2003 and 2017 (59% in 2012, 21% in 2015, 7% in 2003, 6% in 2007, and 3% in 2017).

The average magnitudes of the  $chd32$  trends varied between +0.3 and +1.3 days/10 years (in Dfb and Csa, respectively), and the maximum magnitude of +3.2 days/10 years was obtained in the Csa climate zone. The  $chd32$  maxima by stations varied between 2 and 62 days, with lower values occurring again in coastal and northern stations. The distribution of maxima by years was more heterogeneous compared to the  $nhd32$  (23% in 2012, 21% in 2015, 14% in 1994, 10% in 2007, 9% in 2010, 3% in 2002 and 2003, and few single cases), but EHEs in these years were confirmed by many regional studies [30,33,51,52].

The comparison of multiyear means of  $nhd32$  and  $chd32$  for periods 1961–1990 and 1991–2020 is shown in Figure 4.

**Table 2.** Average/maximum values of Sen’s slope estimates (unit: days/10 years) of statistically significant linear trends ( $p < 0.05$ , Mann-Kendall method) of threshold indicators in the period 1961–2020 by zones of the Köppen–Geiger climate classification; the values  $< 0.1$  days/10 years are not presented; stations’ IDs (see Appendix A, Table A1) are shown in brackets, in which maximum values are reached; percentage of stations with statistically significant trends is also shown.

	Cfa	Cfb	Csa	Dfb
<i>nhd32</i>	+3.8/+7.8 (S10) 100%	+2.4/+5.6 (S24) 100%	+3.7/+8.0 (S56) 93%	+1.0/+3.9 (S57) 93%
<i>chd32</i>	+0.9/+2.8 (S10) 100%	+0.6/+1.3 (S24 and 41) 100%	+1.3/+3.2 (S55) 80%	+0.3/+0.9 (S66) 93%
<i>hsd32</i>	+2.1/+8.7 (S10) 82%	+0.5/+4.4 (S41) 83%	+4.0/+8.1 (S56) 73%	
<i>hsd34</i>	+0.9/+5.6 (S10) 59%	+0.1/+1.6 (S41) 67%	+2.0/+6.2 (S55) 47%	
<i>hsd36</i>	+0.3/+1.7 (S10) 35%		+0.9/+2.7 (S55) 20%	
<i>hsd38</i>				
<i>hsd40</i>				

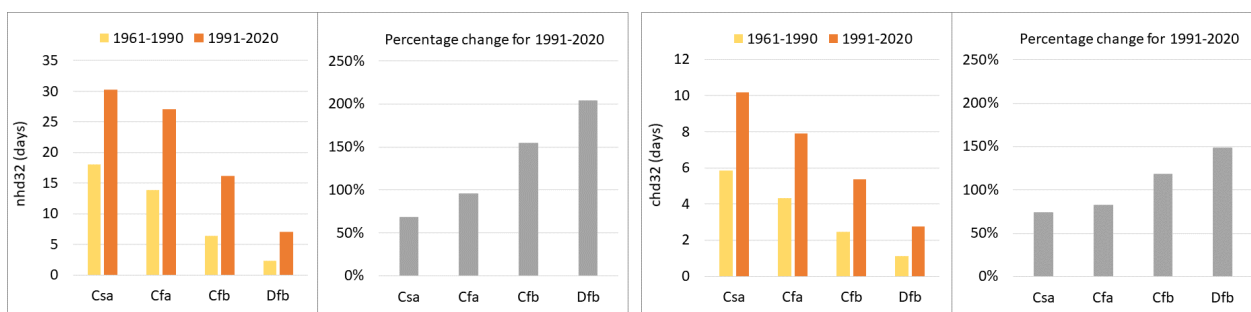


**Figure 4.** Multiyear means of *nhd32* (left panel) and *chd32* (right panel) indicators for periods 1961–1990 and 1991–2020 and percentage changes relative to 1961–1990 by zones of the Köppen–Geiger climate classification.

The number of hot days increased by 12–13 during the second period in the warmer climate zones, reaching about 27–30 days. This result can be viewed in the context of the rapid increase in summer temperatures in Europe, which can lead to month-long spells or even entire seasons with abnormally high temperatures [80]. The largest change for *chd32* in absolute terms (+4.3 days) was registered in the Csa climate zone. Regarding percentage changes, the number of hot days in the cooler climate zones shows the highest increase of about 1.5–2 times during the second period.

Figure 5 presents the evolution of the hot spell duration (*hsd*) indicator by categories, averaged by climate zones. As a whole, the larger *hsd32* is, the higher intensity hot spells can be expected to be, but short, very intense EHEs are also frequent. The highest values for *hsd32* in all climate zones were reached in 2012, followed by 2015; for *hsd34*—in 2012, followed by 2015 (in Cfb and Dfb) and 2007 (in Cfa and Csa); for *hsd36*—2012 (in Cfa and Dfb) and 2007 (in Cfb and Csa); for *hsd38/40*—2007, followed by 2012, 2017, and 2000 (only for *hsd40*). Except for the Mediterranean climate zone Csa, all hot spells at higher categories *hsd38/40*, and almost 90% of the others, emerge after 1985. The average trend magnitudes calculated by the *hsd* categories ranged between +0.1 and +4.0 days/10 years (in Cfb and Csa, respectively), while the maximum magnitude of +8.7 days/10 years was obtained for *hsd32* in the Cfa climate zone (Table 2).

As seen in Table 2, the maximum-trend magnitudes for all indicators were recorded in one or two stations in each climate zone, associated with climate transitions and EHEs’ “hot spots” in SEE [33,81]. These areas are distinguished by a significant increase in the

duration and frequency of hot spells in recent decades. Figure 6 illustrates the detection of “hot spots” by comparing *hsd32* values for the periods 1961–1990 and 1991–2020 by stations.

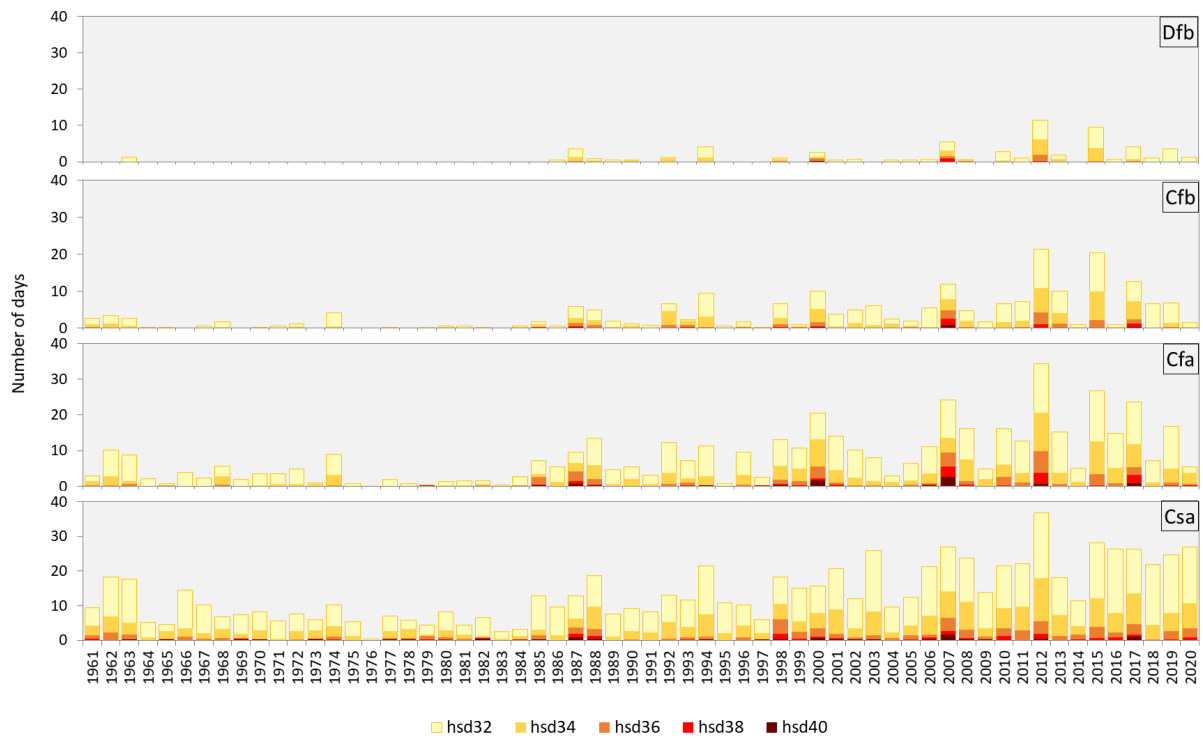


**Figure 5.** Long-term variations of *hsd32/34/36/38/40* (unit: days) averaged by Köppen–Geiger climate zones. In the upper right corner of each panel is shown the 3-letter code of the respective climate zone.

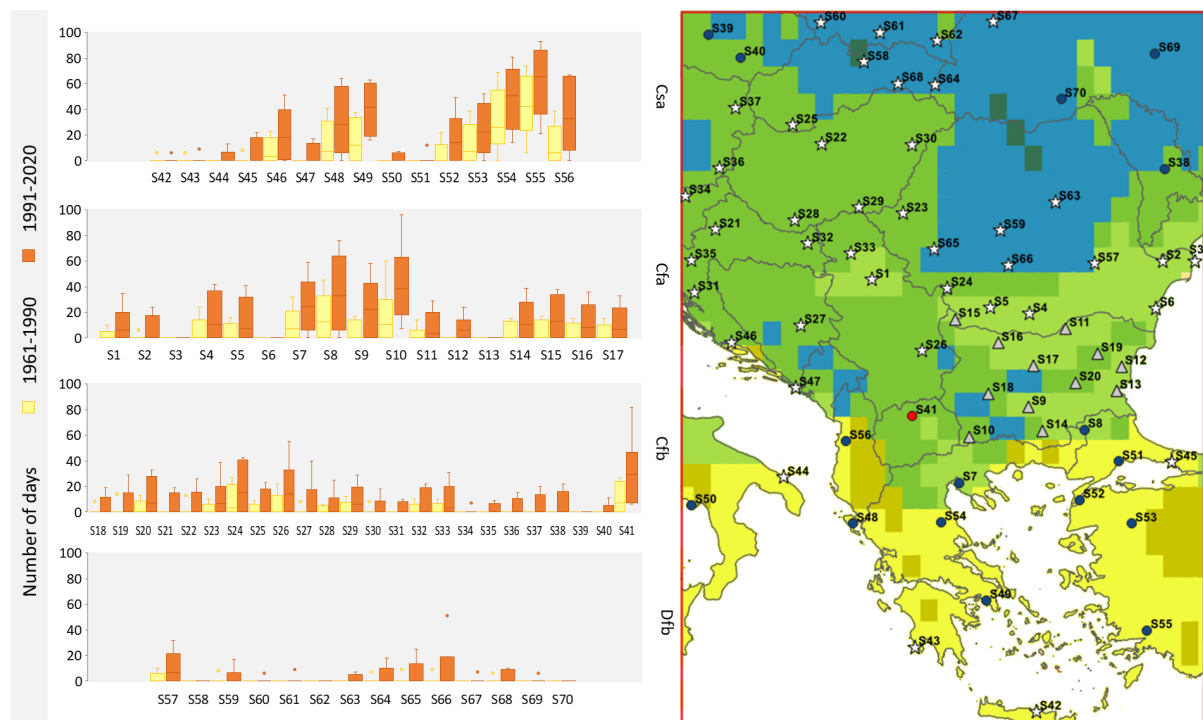


**Figure 6.** Left panel: Box plots of the *hsd32* statistics for the periods 1961–1990 and 1991–2020 by stations grouped by the Köppen–Geiger climate classification zones. Right panel: Location and ID (Appendix A, Table 1) of meteorological stations used in the study on the background of the Köppen–Geiger classification for SEE (see Figure 1).

During the second period, a significant shift in *hsd*<sub>32</sub> statistics is revealed, mainly along the coastal zone in Croatia, Albania, Northern and Central Greece, the Aegean Region in Turkey, and the central part of the Balkan Peninsula. The hottest place in Bulgaria is that between the Struma River Valley and the Kresna Gorge (presented here by S10, Sandanski), where the *hsd* indicator reached maxima for all categories—96 days for *hsd*<sub>32</sub> and 76/46/19/11 days for *hsd*<sub>34/36/38/40</sub>. The duration of individual heat events with *t*<sub>x</sub> ≥ 40 °C reached 6–8 consecutive days [56].

*Comparison between EHF Severity and Categories of hsd Indicator*

The *t*<sub>x</sub>-thresholds that underlie the proposed method for detecting and classifying EHEs by intensity--duration combinations coincide or are very close to some proven physiological thresholds, the crossing of which for a certain time could have significant adverse health and economic consequences. Many regional and worldwide studies have linked the range of daily maximum temperatures of 32–40 °C with an increased risk of worsening and mortality in cardiovascular, respiratory and other illnesses (e.g., [11,12]); agricultural losses [15]; and disruptions in energy production and supply [18]. On the other hand, EHF severity has been shown to be useful as an exposure index that scales well against the human health impact [37], as well as an EHEs indicator in climate studies [82]. Therefore, we choose the EHF<sub>sev</sub> for the suitability assessment of the proposed threshold indicators.

Figure 7 presents the summary estimate of the hot weather in SEE by the mean EHF<sub>sev</sub>, calculated for 1961–1990 and 1991–2020 on a yearly basis over all periods of at least 6 days with *t*<sub>x</sub> ≥ 32 °C (thus being synchronized with the lowest intensity hot spell category *hsd*<sub>32</sub>). The obtained results show that, despite increasing in EHEs in recent decades, the overall warm-season severity remains relatively low in SEE. Percentage changes indicate that the Cfa and Cfb climate zones are more prone to regional warming.

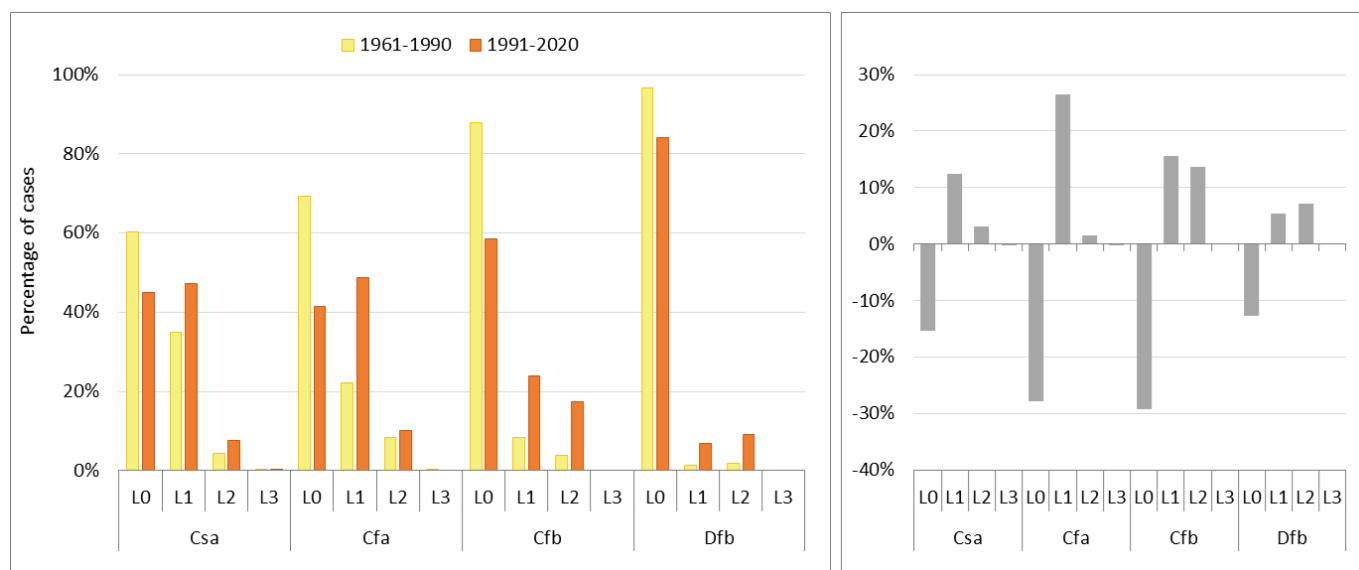


**Figure 7.** Left panel: Mean EHF<sub>sev</sub> across SEE by severity levels according to Nairn et al. [37] for periods 1961–1990 and 1991–2020 by climate zones. Right panel: Percentage change in the mean EHF<sub>sev</sub> for 1991–2020; L0—no extreme heat.

A detailed comparison between the categories of the *hsd* indicator and the levels of the yearly maximum EHF severity demonstrated good spatio-temporal conformity, as seen in Figure 8. For clarity, hot spell categories are denoted by C1 through to C5. Although the correspondence between the categories and the EHF<sub>sev</sub> levels is not straightforward, the percentage distribution of different categories by severity levels shows that the *hsd* indicator significantly underestimates the severity of low-intensity hot spells (C1 category) but tends to overestimate the severity of high-intensity events (C4 category). The me-

dian and minimum value of the averaged *hsd32* metric increase relative to the prevailing severity level.

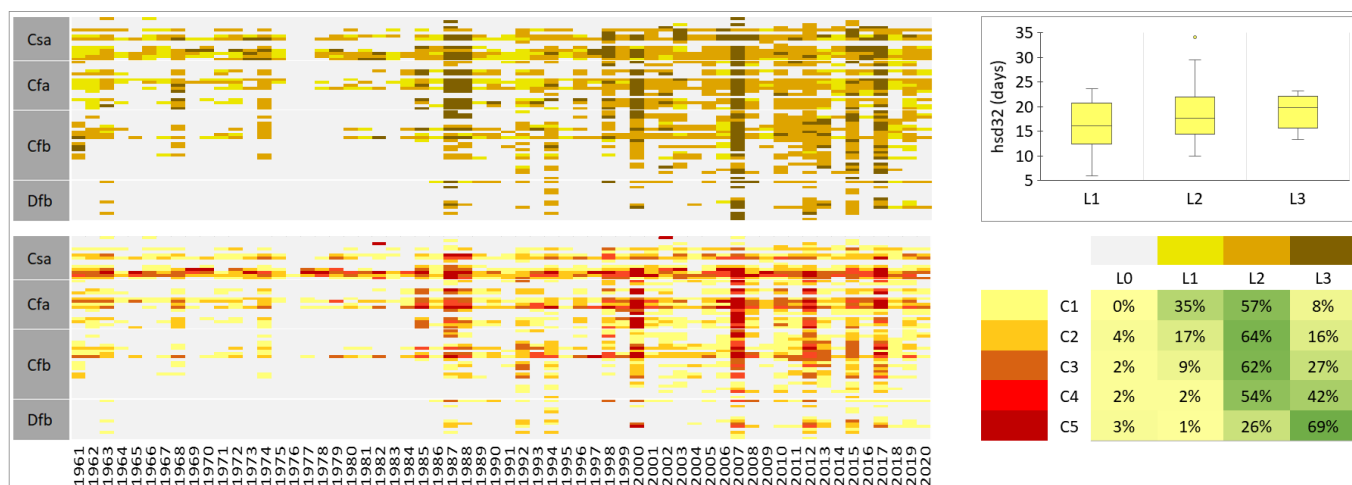


**Figure 8.** Left panel: Spatio-temporal variation of yearly maximum EHEs intensity represented by categories of *hsd* indicator and EHF<sub>sev</sub> levels. Right upper panel: Distribution of *hsd32* values by EHF<sub>sev</sub> levels. Right lower panel: Percentage of different hot spells categories (C1–C5) associated with EHF<sub>sev</sub> levels (L0–L3).

### 5. Conclusions

In this study, daily maximum and minimum air temperature data from 70 selected meteorological stations, which cover the SEE domain relatively evenly, were used to investigate the spatio-temporal variations of extreme heat events in the period 1961–2020. Three threshold-based indicators, quantifying the unfavorable daytime thermal conditions (*nhd32*), the hot weather persistence *chd32*, and the intensity of EHEs in five categories (*hsd32/34/36/38/40*), were analyzed and summarized using the zones of the Köppen–Geiger climate classification. All three indicators show statistically significant linear trends ( $p < 0.05$ , Mann–Kendall method) in the period 1961–2020. The number of hot days increased by 12–13 during the period 1991–2020 in the Cfa and Csa climate zones, reaching about 27–30 days. Both indicators, *nhd32* and *chd32*, show a stronger worsening of daytime thermal conditions in the areas with hot summers.

Many worldwide and regional studies have linked the range of the daily maximum temperature of 32–40 °C with the increased risk of worsening and mortality in cardiovascular, respiratory and other illnesses; agricultural losses; and disruptions in energy production and supply. We demonstrated the suitability of the *tx*-thresholds (32, 34, 36, 38, and 40 °C) and the corresponding duration thresholds (6, 5, 4, 3, and 2 consecutive days) to classify EHEs. Except for the Mediterranean climate zone Csa, all hot spells at higher categories *hsd38/40*, and almost 90% of the others, emerge after 1985. During the period 1991–2020, a significant shift in *hsd32* statistics is recorded in “hot spots”, mainly along the coastal zone in Croatia, Albania, Northern and Central Greece, the Aegean Region in Turkey, and the central part of the Balkan Peninsula. A detailed comparison between the categories of the *hsd* indicator and the levels of the yearly maximum EHF severity demonstrated good spatio-temporal conformity.

As far as we know, such a survey on the various aspects of using threshold indicators for a quantitative assessment of EHEs in the considered region of SEE has not been conducted until now. This research also informs the direction of our next work on the possibilities of a combined application of independently defined metrics, such as the threshold indicators and the EHF index presented here, in climate analyses and the implementation of the obtained knowledge in early warning systems.

**Author Contributions:** Conceptualization, K.M. and H.C.; methodology, K.M.; software, K.M. and H.C.; validation, K.M. and L.B.; resources, L.B. and H.C.; data curation, K.M.; writing—original draft preparation, K.M.; writing—review and editing, K.M. and H.C.; visualization, K.M. All authors have read and agreed to the published version of the manuscript.

**Funding:** This research received no external funding.

**Institutional Review Board Statement:** Not applicable.

**Informed Consent Statement:** Not applicable

**Data Availability Statement:** Not applicable.

**Acknowledgments:** Due to the fact that this study is entirely based on free available data and software, the authors would like to express their deep gratitude to all organizations and institutions (ECA&D, NCDC, NCEI, ECMWF, the R Core and QGIS teams, MPI-M, and others) which provides free-of-charge software and data. Not least, we thank the three anonymous reviewers for their valuable comments and suggestions which led to an overall improvement of the original manuscript.

**Conflicts of Interest:** The authors declare no conflict of interest.

## Appendix A. Data

**Table A1.** Key information for the 12 selected stations from the NIMH network, 41 selected stations from the ECA&D database, 16 selected stations from the GHCNd dataset, and one station from the GSOD dataset; KGC denotes the Köppen–Geiger climate classification.

Station ID	Station Name	Country Code (ISO 3166-1)	Latitude (N)	Longitude (E)	Altitude (m)	Data Source	KGC	Environment
S1	Belgrade (Obs.)	RS	44.8	20.4667	132	ECA&D	Cfa	urban
S2	Tulcea	RO	45.1831	28.8167	4	ECA&D	Cfa	suburban
S3	Sulina	RO	45.1667	29.7331	3	ECA&D	Cfa	rural
S4	Roşiorii de Vede	RO	44.1	24.9831	102	ECA&D	Cfa	rural
S5	Craiova	RO	44.23	23.87	192	ECA&D	Cfa	rural
S6	Constanța	RO	44.22	28.63	13	ECA&D	Cfa	suburban
S7	Thessaloniki Airport	GR	40.52	22.97	7	GHCNd	Cfa	airport
S8	Edirne	TR	41.67	26.57	51	GHCNd	Cfa	urban
S9	Sadovo	BG	42.15	24.95	155	NIMH	Cfa	rural
S10	Sandanski	BG	41.52	23.27	206	NIMH	Cfa	suburban
S11	Obraztsov Chiflik	BG	43.8	26.0331	156	NIMH	Cfa	suburban
S12	Goren Chiflik	BG	43.0094	27.6297	29	NIMH	Cfa	suburban
S13	Burgas	BG	42.4977	27.4827	22	NIMH	Cfa	suburban
S14	Kardzhali	BG	41.65	25.37	331	NIMH	Cfa	suburban
S15	Vidin	BG	43.9942	22.8525	31	NIMH	Cfa	suburban
S16	Knezha	BG	43.5	24.0831	116	NIMH	Cfa	rural
S17	Sevlievo	BG	43.0256	25.1151	197	NIMH	Cfa	suburban
S18	Ihtiman	BG	42.4381	23.8196	637	NIMH	Cfb	urban
S19	Shumen	BG	43.2796	26.944	217	NIMH	Cfb	suburban
S20	Sliven	BG	42.6776	26.3398	259	NIMH	Cfb	urban
S21	Zagreb- Grič	HR	45.8167	15.9781	156	ECA&D	Cfb	urban
S22	Budapest	HU	47.5108	19.0206	153	ECA&D	Cfb	urban
S23	Arad	RO	46.1331	21.35	116	ECA&D	Cfb	suburban
S24	Drobeta-Turnu Severin	RO	44.6331	22.6331	77	ECA&D	Cfb	suburban
S25	Hurbanovo	SK	47.8667	18.1831	115	ECA&D	Cfb	suburban
S26	Niš	RS	43.3331	21.9	201	ECA&D	Cfb	suburban
S27	Sarajevo	BA	43.8678	18.4228	630	ECA&D	Cfb	urban
S28	Pécs-Pogány	HU	46.0056	18.2328	202	ECA&D	Cfb	airport
S29	Szeged	HU	46.2558	20.0903	81	ECA&D	Cfb	suburban

Table A1. Cont.

Station ID	Station Name	Country Code (ISO 3166-1)	Latitude (N)	Longitude (E)	Altitude (m)	Data Source	KGC	Environment
S30	Debrecen Airport	HU	47.4903	21.6106	107	ECA&D	Cfb	airport
S31	Gospić	HR	44.55	15.3667	564	ECA&D	Cfb	suburban
S32	Osijek	HR	45.5331	18.6331	88	ECA&D	Cfb	suburban
S33	Novi Sad	RS	45.3331	19.85	84	ECA&D	Cfb	suburban
S34	Šmartno pri Gradcu	SI	46.4894	15.1108	444	ECA&D	Cfb	rural
S35	Ogulin	HR	45.2039	15.2717	326	ECA&D	Cfb	rural
S36	Fürstenfeld	AT	47.0308	16.0806	323	ECA&D	Cfb	rural
S37	Gross-Enzersdorf	AT	48.1994	16.5589	154	ECA&D	Cfb	suburban
S38	Kisinev	MD	47.02	28.87	173	GHCNd	Cfb	urban
S39	Přibyslav	CZ	49.5828	15.7625	532	GHCNd	Cfb	rural
S40	Brno-Tuřany	CZ	49.1531	16.6889	241	GHCNd	Cfb	airport
S41	Skopje International Airport	MK	41.9616	21.6214	238	GSOD	Cfb	airport
S42	Heraklion	GR	35.3331	25.1831	39	ECA&D	Csa	airport
S43	Methoni	GR	36.8331	21.7	51	ECA&D	Csa	rural
S44	Brindisi	IT	40.6331	17.9331	10	ECA&D	Csa	urban
S45	Istanbul	TR	40.9667	29.0831	33	ECA&D	Csa	urban
S46	Split Marjan	HR	43.5167	16.4331	122	ECA&D	Csa	urban
S47	Dubrovnik	HR	42.56	18.27	52	ECA&D	Csa	urban
S48	Corfu	GR	39.62	19.92	11	GHCNd	Csa	urban
S49	Hellinikon	GR	37.9	23.75	10	GHCNd	Csa	urban
S50	Cape Palinuro	IT	40.0251	15.2805	185	GHCNd	Csa	rural
S51	Tekirdag	TR	40.98	27.55	3	GHCNd	Csa	urban
S52	Çanakkale	TR	40.14	26.43	7	GHCNd	Csa	airport
S53	Balikesir	TR	39.62	27.93	104	GHCNd	Csa	airport
S54	Larissa	GR	39.65	22.45	73	GHCNd	Csa	airport
S55	Mugla	TR	37.22	28.37	646	GHCNd	Csa	urban
S56	Tirana	AL	41.3333	19.7833	38	GHCNd	Csa	urban
S57	Buzau	RO	45.1331	26.85	97	ECA&D	Dfb	suburban
S58	Poprad-Tatry	SK	49.0667	20.2331	694	ECA&D	Dfb	airport
S59	Sibiu	RO	45.8	24.15	444	ECA&D	Dfb	airport
S60	Bielsko-Biala	PL	49.8069	19.0003	396	ECA&D	Dfb	suburban
S61	Nowy Sącz	PL	49.6272	20.6886	292	ECA&D	Dfb	suburban
S62	Lesko	PL	49.4664	22.3417	420	ECA&D	Dfb	suburban
S63	Miercurea Ciuc	RO	46.3667	25.7331	661	ECA&D	Dfb	rural
S64	Uzhhorod	UA	48.6331	22.2667	124	ECA&D	Dfb	suburban
S65	Caransebeș	RO	45.42	22.25	241	ECA&D	Dfb	airport
S66	Râmnicu Vâlcea	RO	45.1	24.37	239	ECA&D	Dfb	urban
S67	Lviv	UA	49.8167	23.95	323	ECA&D	Dfb	urban
S68	Košice	SK	48.6667	21.2167	230	ECA&D	Dfb	airport
S69	Vynnytsia	UA	49.23	28.6	298	GHCNd	Dfb	airport
S70	Chernivtsi	UA	48.3667	25.9	246	GHCNd	Dfb	rural

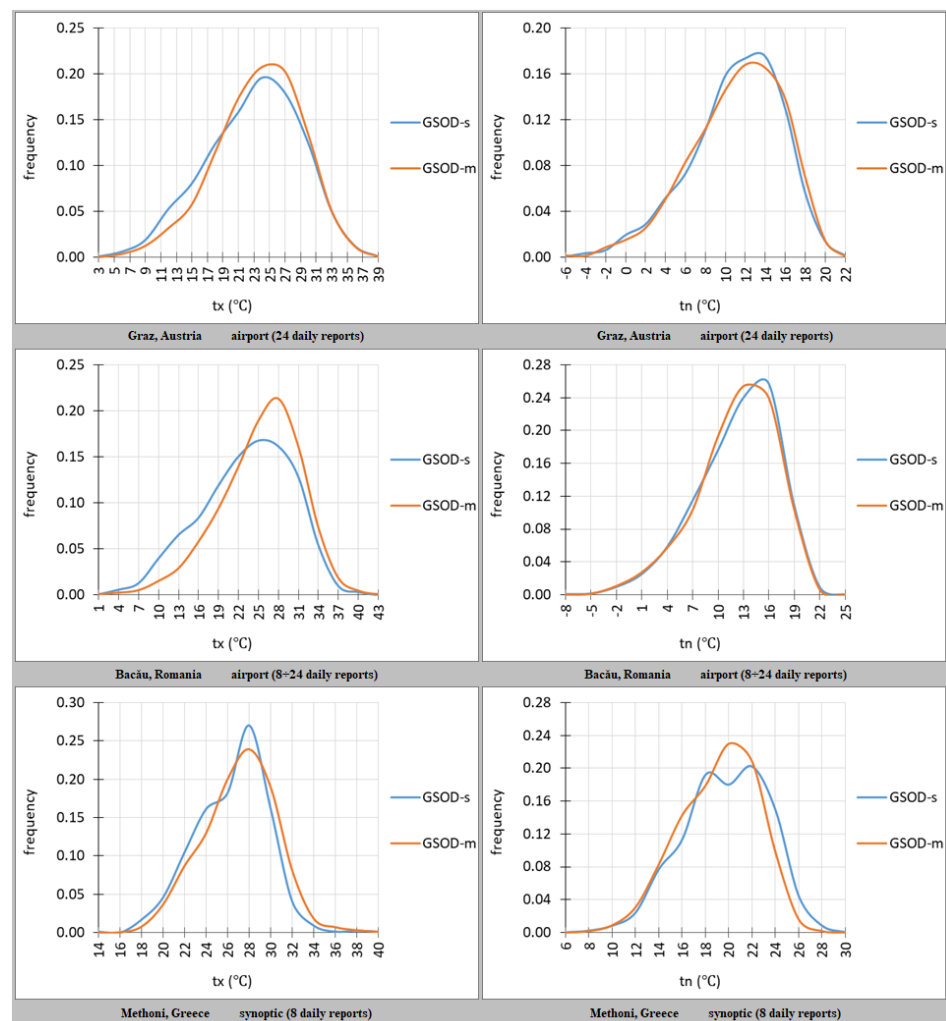


**Figure A1.** Comparison between samples of measured maximum/minimum temperatures (GSOD-m) and substituted maximum/minimum temperatures (GSOD-s) for the warm half year (May–October) by stations with different climates, environments, and observational routines;  $tx$ —daily maximum temperature,  $tn$ —daily minimum temperature.

### Appendix B. Iterative PCA Imputation Technique Using the R-Package ‘MissMDA’

The PCA-based spatio-temporal reconstruction of time series was performed over the grouped by regions stations based on the Köppen–Geiger climate classification and correlation between stations’ data. For each station with medium to large data gaps, the data extracted from the ERA5-Land spatio-temporally coherent time series were also included to improve the quality of the imputation process. Firstly, the number of principal components that should be used to replace missing values was determined using the ‘estim\_ncpPCA’ function, which applies a generalized cross-validation approach to attain the smallest mean square error of prediction. Data were then reconstructed from the principal components by the ‘imputePCA’ function, which automates the imputation process, and the missing values in the original data were ultimately replaced with estimates from the last PCA data reconstruction (Figure A2). The average NRMSE (Normalized Root Mean Squared Error,  $NRMSE = RMSE/SD(O)$ , where  $SD(O)$  denotes the standard deviation of the time series before reconstruction), for the minimum temperatures is around 13% (from 7.5% to 18.6%), and for the maximum temperatures, it is approximately 10% (from 5.5% to 13%).

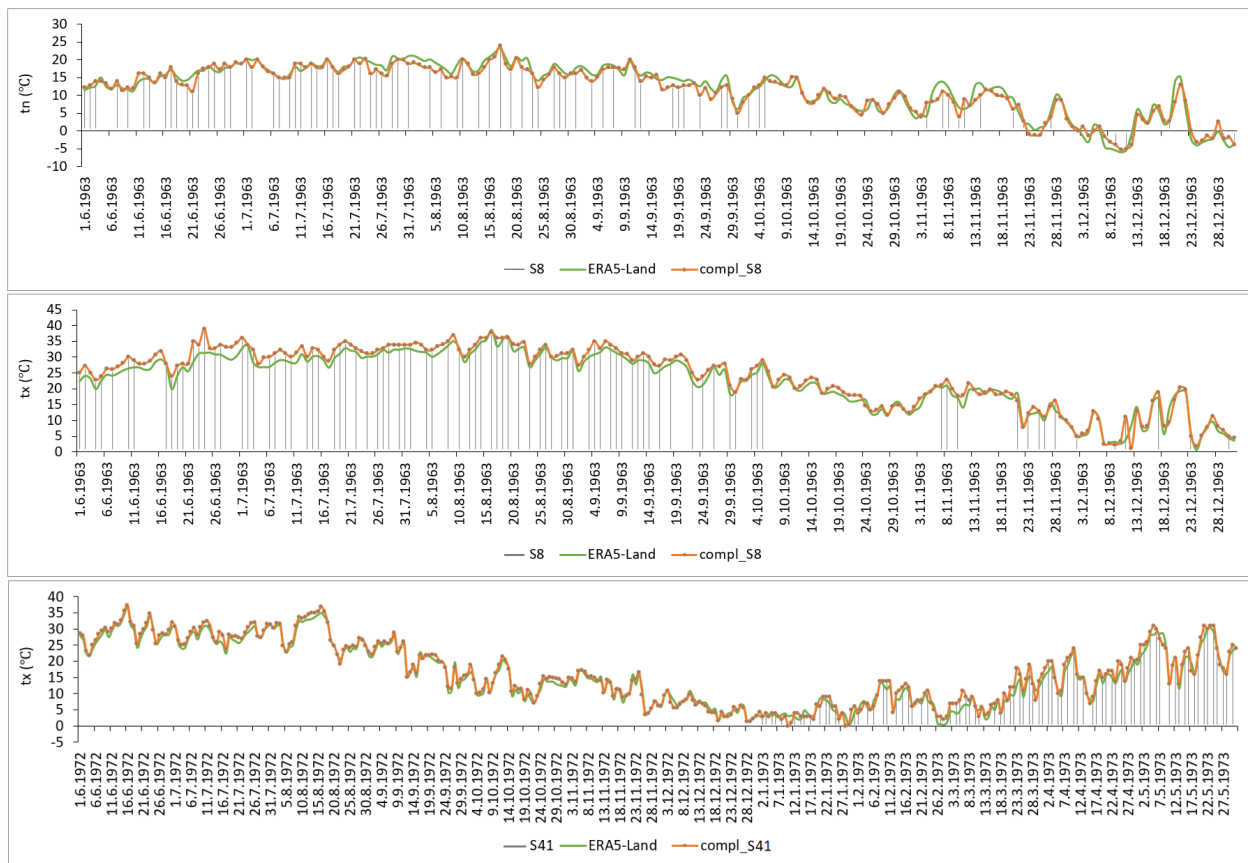


**Figure A2.** Upper panel: Missing values ( $tn$ ) imputation in the case of small to medium gaps number (Edirne). Middle panel: Missing values ( $tx$ ) imputation in the case of small to medium gaps number (Edirne). Lower panel: Missing values ( $tx$ ) extrapolation (Skopje International Airport).  $tx$ —daily maximum temperature,  $tn$ —daily minimum temperature.

### Appendix C. Defining Hot Spells Duration Indicator ( $hsd_{32/34/36/38/40}$ )

Statistical modeling of hot-weather phenomena involved several steps: (1) the construction of empirical distributions of maximum temperatures in July and August from the selected 36 stations for 1931–1980 (the period is considered to be less affected by global warming [2,4,83]); the calculation of return levels corresponds to return periods 2, 5, 10, 20, and 50 years using the Generalized Extreme Value (GEV) distribution, (3) determination of appropriate thresholds for  $tx$ ; (4) determination of hot spell duration thresholds for the period 1961–2019 at the different  $tx$ -thresholds; (5) validation of obtained thresholds for the period 1961–2019. The estimated  $tx$ -threshold values are 32, 34, 36, 38, and 40 °C, and the relevant hot spells duration thresholds are 6, 5, 4, 3, and 2 consecutive days.

In the period 1931–1980, the daily maximum temperatures ( $tx$ ) of July and August in the selected stations fall most often into the range 26–31 °C, and the absolute maxima are typically between 38 °C and 41 °C. During the second period (1981–2019), a significant shift of  $tx$ -distributions toward higher values is observed (Figure A3, left panel). In order to provide a reliable analysis for the period 1961–2019, the temperature thresholds were determined using statistical modeling, not from the upper-tail percentiles of the empirical distributions for 1931–1980 (Figure A3, middle panel). From the estimated 2-, 5-, 10-, 20-, and 50-year return levels of maximum July–August temperatures by the GEV model, thresholds have been chosen in such a way as to be achievable in 85–90% of stations for the shorter return periods and in 50–60% of stations—for the longer ones. The right panel of Figure A3 presents the percentiles of hot spell durations at different  $tx$ -thresholds in the period 1961–2019. Hot weather lasts 1–3 days most frequently, and the 90th percentile varies between 3 and 6 days.

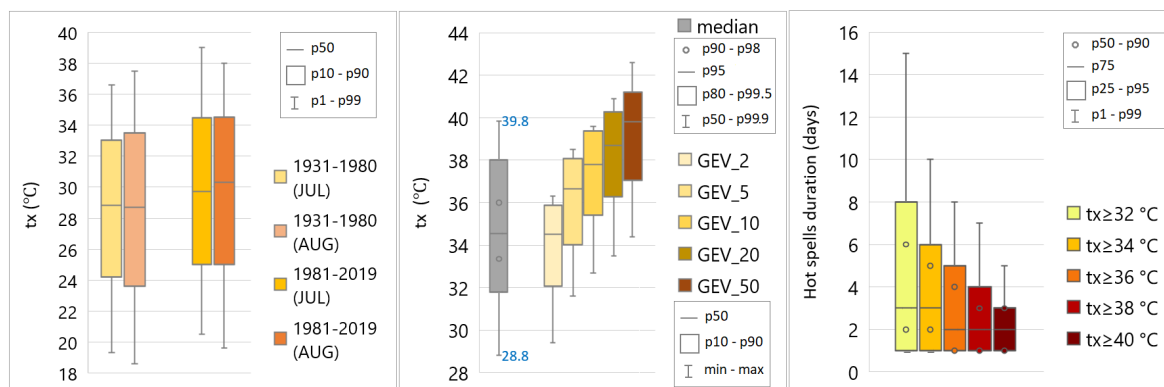


**Figure A3.** Left panel: Medians of calculated percentiles of  $tx$ -distributions by stations for 1931–1980 and 1981–2019. Middle panel: Median of calculated upper percentiles of  $tx$ -distributions and 2-, 5-, 10-, 20-, and 50-year return levels (estimated by GEV model) by stations for July–August (1931–1980). Right panel: Box plot of distributions of hot spells duration at the different  $tx$ -thresholds for 1961–2019.

### Appendix D. Description of EHF Index Calculation

The EHF is a measure of heatwave intensity, incorporating two ingredients [76,84]. The first ingredient ( $E_{sig}$ ) is a measure of how hot a three-day period is with respect to the 95th percentile of the daily mean temperature at each particular location. The percentile is computed for a reference period of 30 years (1961–1990 in our study) using the daily mean temperatures for all days in the year. The second ingredient ( $E_{accl}$ ) is a measure of how hot the three-day period is with respect to the recent past (specifically the previous 30 days). This takes into account the idea that people acclimatize to their local climate, with respect to its temperature variation across latitudes and throughout the year, but may not be prepared for a sudden rise in temperature above that of the recent past. We used the retrospective version of equations for the three-day mean temperature (over days  $i$  to  $i - 2$ ):

$$EHI_{sigi} = (T_i + T_{i-1} + T_{i-2}) - T_{95}, \tag{A1}$$

$$EHI_{accli} = (T_i + T_{i-1} + T_{i-2}) - (T_{i-3} + \dots + T_{i-32})/30, \text{ and} \tag{A2}$$

$$T_i = (T_{maxi} + T_{mini})/2, \tag{A3}$$

where  $T_i$  denotes the daily mean temperature on day  $i$ ,  $T_{95}$  represents the long-term 95th percentile of the daily mean temperature,  $EHI_{sigi}$  is defined as the exceeding of the previous three-day mean temperature (starting on day  $i$ ) above  $T_{95}$ , and  $EHI_{accli}$  on day  $i$  is calculated as the difference between the three-day mean temperature and a mean of the prior 30 days. Consequently, the daily EHF was calculated using the following equation:

$$EHF_i = EHI_{sigi} \times \max(1, EHI_{accli}). \tag{A4}$$

### References

1. Masson-Delmotte, V.; Zhai, P.; Pirani, A.; Connors, S.; Péan, C.; Berger, S.; Caud, N.; Chen, Y.; Goldfarb, L.; Gomis, M.; et al. Climate Change 2021: The Physical Science Basis. In *Contribution of Working Group I to the Sixth Assessment Report of the Intergovernmental Panel on Climate Change*; Technical Report; IPCC: Geneva, Switzerland, 2021. [CrossRef]
2. WMO. *State of the Global Climate 2021: WMO Provisional Report*; Technical Report; WMO: Geneva, Switzerland, 2021.
3. Randalls, S. History of the 2 °C climate target. *WIREs Clim. Chang.* **2010**, *1*, 598–605. [CrossRef]
4. Cramer, W.; Guiot, J.; Marini, K. *Climate and Environmental Change in the Mediterranean Basin—Current Situation and Risks for the Future*; MedECC: First Mediterranean Assessment Report; Technical Report; UNEP/MAP: Marseille, France, 2020.
5. Vogel, M.M.; Zscheischler, J.; Wartenburger, R.; Dee, D.; Seneviratne, S.I. Concurrent 2018 Hot Extremes Across Northern Hemisphere Due to Human—Induced Climate Change. *Earth Future* **2019**, *7*, 692–703. [CrossRef] [PubMed]
6. Zhang, P.; Jeong, J.H.; Yoon, J.H.; Kim, H.; Wang, S.Y.S.; Linderholm, H.W.; Fang, K.; Wu, X.; Chen, D. Abrupt shift to hotter and drier climate over inner East Asia beyond the tipping point. *Science* **2020**, *370*, 1095–1099. [CrossRef]

7. Diffenbaugh, N.S.; Field, C.B. Changes in Ecologically Critical Terrestrial Climate Conditions. *Science* **2013**, *341*, 486–492. [[CrossRef](#)]
8. Vautard, R.; van Aalst, M.; Boucher, O.; Drouin, A.; Haustein, K.; Kreienkamp, F.; van Oldenborgh, G.J.; Otto, F.E.L.; Ribes, A.; Robin, Y.; et al. Human contribution to the record-breaking June and July 2019 heatwaves in Western Europe. *Environ. Res. Lett.* **2020**, *15*, 094077. [[CrossRef](#)]
9. WMO. *Atlas of Mortality and Economic Losses from Weather, Climate and Water Extremes (1970–2019)*; Technical Report; WMO: Geneva, Switzerland, 2021.
10. Sheridan, S.C.; Allen, M.J. Temporal trends in human vulnerability to excessive heat. *Environ. Res. Lett.* **2018**, *13*, 043001. [[CrossRef](#)]
11. Petitti, D.B.; Hondula, D.M.; Yang, S.; Harlan, S.L.; Chowell, G. Multiple Trigger Points for Quantifying Heat-Health Impacts: New Evidence from a Hot Climate. *Environ. Health Perspect.* **2016**, *124*, 176–183. [[CrossRef](#)] [[PubMed](#)]
12. Li, J.; Xu, X.; Yang, J.; Liu, Z.; Xu, L.; Gao, J.; Liu, X.; Wu, H.; Wang, J.; Yu, J.; et al. Ambient high temperature and mortality in Jinan, China: A study of heat thresholds and vulnerable populations. *Environ. Res.* **2017**, *156*, 657–664. [[CrossRef](#)]
13. Deryugina, T.; Hsiang, S. *Does the Environment Still Matter? Daily Temperature and Income in the United States*; Technical Report w20750; National Bureau of Economic Research: Cambridge, MA, USA, 2014. [[CrossRef](#)]
14. García-León, D.; Casanueva, A.; Standardi, G.; Burgstall, A.; Flouris, A.D.; Nybo, L. Current and projected regional economic impacts of heatwaves in Europe. *Nat. Commun.* **2021**, *12*, 5807. [[CrossRef](#)]
15. Teixeira, E.I.; Fischer, G.; van Velthuizen, H.; Walter, C.; Ewert, F. Global hot-spots of heat stress on agricultural crops due to climate change. *Agric. For. Meteorol.* **2013**, *170*, 206–215. [[CrossRef](#)]
16. Grotjahn, R. Weather Extremes That Affect Various Agricultural Commodities. In *Extreme Events and Climate Change*, 1st ed.; Castillo, F., Wehner, M., Stone, D.A., Eds.; Wiley: Hoboken, NJ, USA, 2021; pp. 21–48. [[CrossRef](#)]
17. Lass, W.; Haas, A.; Hinkel, J.; Jaeger, C. Avoiding the avoidable: Towards a European heatwaves risk governance. *Int. J. Disaster Risk Sci.* **2011**, *2*, 1–14. [[CrossRef](#)]
18. Añel, J.; Fernández-González, M.; Labandeira, X.; López-Otero, X.; de la Torre, L. Impact of Cold Waves and Heat Waves on the Energy Production Sector. *Atmosphere* **2017**, *8*, 209. [[CrossRef](#)]
19. Sun, Q.; Miao, C.; Hanel, M.; Borthwick, A.G.; Duan, Q.; Ji, D.; Li, H. Global heat stress on health, wildfires, and agricultural crops under different levels of climate warming. *Environ. Int.* **2019**, *128*, 125–136. [[CrossRef](#)] [[PubMed](#)]
20. Spinoni, J.; Vogt, J.V.; Barbosa, P.; Dosio, A.; McCormick, N.; Bigano, A.; Füssler, H.M. Changes of heating and cooling degree-days in Europe from 1981 to 2100: HDD and CDD in Europe from 1981 to 2100. *Int. J. Climatol.* **2018**, *38*, e191–e208. [[CrossRef](#)]
21. Morabito, M.; Crisci, A.; Messeri, A.; Messeri, G.; Betti, G.; Orlandini, S.; Raschi, A.; Maracchi, G. Increasing Heatwave Hazards in the Southeastern European Union Capitals. *Atmosphere* **2017**, *8*, 115. [[CrossRef](#)]
22. Russo, S.; Sillmann, J.; Fischer, E.M. Top ten European heatwaves since 1950 and their occurrence in the coming decades. *Environ. Res. Lett.* **2015**, *10*, 124003. [[CrossRef](#)]
23. Beniston, M. The 2003 heat wave in Europe: A shape of things to come? An analysis based on Swiss climatological data and model simulations. *Geophys. Res. Lett.* **2004**, *31*. [[CrossRef](#)]
24. Sánchez-Benítez, A.; García-Herera, R.; Barriopedro, D.; Sousa, P.M.; Trigo, R.M. June 2017: The Earliest European Summer Mega-heatwave of Reanalysis Period. *Geophys. Res. Lett.* **2018**, *45*, 1955–1962. [[CrossRef](#)]
25. Schär, C.; Vidale, P.L.; Lüthi, D.; Frei, C.; Häberli, C.; Liniger, M.A.; Appenzeller, C. The role of increasing temperature variability in European summer heatwaves. *Nature* **2004**, *427*, 332–336. [[CrossRef](#)]
26. Xoplaki, E.; Trigo, R.M.; García-Herera, R.; Barriopedro, D.; D’Andrea, F.; Fischer, E.M.; Gimeno, L.; Gouveia, C.; Hernández, E.; Kuglitsch, F.G.; et al. Large-Scale Atmospheric Circulation Driving Extreme Climate Events in the Mediterranean and its Related Impacts. In *The Climate of the Mediterranean Region*; Elsevier: Amsterdam, The Netherlands, 2012; pp. 347–417. [[CrossRef](#)]
27. Diffenbaugh, N.S.; Pal, J.S.; Giorgi, F.; Gao, X. Heat stress intensification in the Mediterranean climate change hotspot. *Geophys. Res. Lett.* **2007**, *34*, L11706. [[CrossRef](#)]
28. Della-Marta, P.M.; Luterbacher, J.; von Weissenfluh, H.; Xoplaki, E.; Brunet, M.; Wanner, H. Summer heatwaves over western Europe 1880–2003, their relationship to large-scale forcings and predictability. *Clim. Dyn.* **2007**, *29*, 251–275. [[CrossRef](#)]
29. Kuglitsch, F.G.; Toreti, A.; Xoplaki, E.; Della-Marta, P.M.; Zerefos, C.S.; Türkeş, M.; Luterbacher, J. Heat wave changes in the eastern Mediterranean since 1960. *Geophys. Res. Lett.* **2010**, *37*. [[CrossRef](#)]
30. Tolika, K. Assessing Heat Waves over Greece Using the Excess Heat Factor (EHF). *Climate* **2019**, *7*, 9. [[CrossRef](#)]
31. Horton, R.M.; Mankin, J.S.; Lesk, C.; Coffel, E.; Raymond, C. A Review of Recent Advances in Research on Extreme Heat Events. *Curr. Clim. Chang. Rep.* **2016**, *2*, 242–259. [[CrossRef](#)]
32. Kotteck, M.; Grieser, J.; Beck, C.; Rudolf, B.; Rubel, F. World Map of the Köppen-Geiger climate classification updated. *Meteorol. Z.* **2006**, *15*, 259–263. [[CrossRef](#)]
33. Lionello, P.; Abrantes, F.; Congedi, L.; Dulac, F.; Gacic, M.; Gomis, D.; Goodess, C.; Hoff, H.; Kutiel, H.; Luterbacher, J.; et al. Introduction: Mediterranean Climate—Background Information. In *The Climate of the Mediterranean Region*; Elsevier: Amsterdam, The Netherlands, 2012. [[CrossRef](#)]
34. Perkins, S.E. A review on the scientific understanding of heatwaves—Their measurement, driving mechanisms, and changes at the global scale. *Atmos. Res.* **2015**, *164–165*, 242–267. [[CrossRef](#)]

35. Russo, S.; Dosio, A.; Graversen, R.G.; Sillmann, J.; Carrao, H.; Dunbar, M.B.; Singleton, A.; Montagna, P.; Barbola, P.; Vogt, J.V. Magnitude of extreme heatwaves in present climate and their projection in a warming world. *J. Geophys. Res. Atmos.* **2014**, *119*, 12500–12512. [[CrossRef](#)]
36. Perkins, S.E.; Alexander, L.V. On the Measurement of Heat Waves. *J. Clim.* **2013**, *26*, 4500–4517. [[CrossRef](#)]
37. Nairn, J.; Ostendorf, B.; Bi, P. Performance of Excess Heat Factor Severity as a Global Heatwave Health Impact Index. *Int. J. Environ. Res. Public Health* **2018**, *15*, 2494. [[CrossRef](#)]
38. Casanueva, A.; Burgstall, A.; Kotlarski, S.; Messeri, A.; Morabito, M.; Flouris, A.D.; Nybo, L.; Spirig, C.; Schwierz, C. Overview of Existing Heat-Health Warning Systems in Europe. *Int. J. Environ. Res. Public Health* **2019**, *16*, 2657. [[CrossRef](#)]
39. Tong, S.; Wang, X.Y.; Barnett, A.G. Assessment of Heat-Related Health Impacts in Brisbane, Australia: Comparison of Different Heatwave Definitions. *PLoS ONE* **2010**, *5*, e12155. [[CrossRef](#)]
40. Sulikowska, A.; Wypych, A. Summer temperature extremes in Europe: How does the definition affect the results? *Theor. Appl. Climatol.* **2020**, *141*, 19–30. [[CrossRef](#)]
41. Di Napoli, C.; Pappenberger, F.; Cloke, H.L. Assessing heat-related health risk in Europe via the Universal Thermal Climate Index (UTCI). *Int. J. Biometeorol.* **2018**, *62*, 1155–1165. [[CrossRef](#)]
42. Matzarakis, A.; Laschewski, G.; Muthers, S. The Heat Health Warning System in Germany—Application and Warnings for 2005 to 2019. *Atmosphere* **2020**, *11*, 170. [[CrossRef](#)]
43. Dunn, R.J.H.; Alexander, L.V.; Donat, M.G.; Zhang, X.; Bador, M.; Herold, N.; Lippmann, T.; Allan, R.; Aguilar, E.; Barry, A.A.; et al. Development of an Updated Global Land In Situ-Based Data Set of Temperature and Precipitation Extremes: HadEX3. *J. Geophys. Res. Atmos.* **2020**, *125*, e2019JD032263. [[CrossRef](#)]
44. Donat, M.; Alexander, L.; Yang, H.; Durre, I.; Vose, R.; Caesar, J. Global Land-Based Datasets for Monitoring Climatic Extremes. *Bull. Am. Meteorol. Soc.* **2013**, *94*, 997–1006. [[CrossRef](#)]
45. Di Napoli, C.; Barnard, C.; Prudhomme, C.; Cloke, H.L.; Pappenberger, F. ERA5-HEAT: A global gridded historical dataset of human thermal comfort indices from climate reanalysis. *Geosci. Data J.* **2021**, *8*, 2–10. [[CrossRef](#)]
46. Raei, E.; Nikoo, M.R.; AghaKouchak, A.; Mazdiyasi, O.; Sadegh, M. GHWR, a multi-method global heatwave and warm-spell record and toolbox. *Sci. Data* **2018**, *5*, 180206. [[CrossRef](#)]
47. Domínguez-Castro, F.; Reig, F.; Vicente-Serrano, S.M.; Aguilar, E.; Peña-Angulo, D.; Noguera, I.; Revuelto, J.; van der Schrier, G.; El Kenawy, A.M. A multidecadal assessment of climate indices over Europe. *Sci. Data* **2020**, *7*, 125. [[CrossRef](#)]
48. Chervenkov, H.; Slavov, K.; Ivanov, V. STARDEX and ETCCDI climate indices based on E-OBS and CARPATCLIM part one: General description. In *Numerical Methods and Applications*; Nikolov, G., Kolkovska, N., Georgiev, K., Eds.; Springer: Cham, Switzerland, 2019; Volume 11189, pp. 360–367.
49. Urban, A.; Kyselý, J. Comparison of UTCI with other thermal indices in the assessment of heat and cold effects on cardiovascular mortality in the Czech Republic. *Int. J. Environ. Res. Public Health* **2014**, *11*, 952–967. [[CrossRef](#)]
50. Founda, D.; Giannakopoulos, C. The exceptionally hot summer of 2007 in Athens, Greece—A typical summer in the future climate? *Glob. Planet. Chang.* **2009**, *67*, 227–236. [[CrossRef](#)]
51. Pecelj, M.M.; Lukić, M.Z.; Filipović, D.J.; Protić, B.M.; Bogdanović, U.M. Analysis of the universal thermal climate index during heatwaves in Serbia. *Nat. Hazards Earth Syst. Sci.* **2020**, *20*, 2021–2036. [[CrossRef](#)]
52. Urban, A.; Hanzlíková, H.; Kyselý, J.; Plavcová, E. Impacts of the 2015 heatwaves on mortality in the Czech Republic—A comparison with previous heatwaves. *Int. J. Environ. Res. Public Health* **2017**, *14*, 1562. [[CrossRef](#)]
53. Piticar, A.; Croitoru, A.E.; Ciupertea, F.A.; Harpa, G.V. Recent changes in heatwaves and cold waves detected based on excess heat factor and excess cold factor in Romania: Changes in heat wave and cold wave indices in Romania. *Int. J. Climatol.* **2018**, *38*, 1777–1793. [[CrossRef](#)]
54. Katavoutas, G.; Founda, D. Response of urban heat stress to heatwaves in Athens (1960–2017). *Atmosphere* **2019**, *10*, 483. [[CrossRef](#)]
55. Gocheva, A.; Malcheva, K. Extremely hot spells on the territory of Bulgaria. *Bulg. J. Meteorol. Hydrol.* **2010**, *15*, 64–81.
56. Malcheva, K.; Bocheva, L.; Chervenkov, H. Climatology of extremely hot spells in Bulgaria (1961–2019). In *Proceedings of the 21st International Multidisciplinary Scientific GeoConference SGEM 2021, STEF92 Technology, Sofia, Bulgaria, 16–22 August 2021*; Trofymchuk, O., Rivza, B., Eds.; Volume 21, pp. 237–244. [[CrossRef](#)]
57. Klein Tank, A.M.G.; Wijngaard, J.B.; Können, G.P.; Böhm, R.; Demarée, G.; Gocheva, A.; Miletta, M.; Pashiardis, S.; Hejkrlik, L.; Kern-Hansen, C.; et al. Daily dataset of 20th-century surface air temperature and precipitation series for the European Climate Assessment. *Int. J. Climatol.* **2002**, *22*, 1441–1453. [[CrossRef](#)]
58. Menne, M.J.; Durre, I.; Vose, R.S.; Gleason, B.E.; Houston, T.G. An Overview of the Global Historical Climatology Network-Daily Database. *J. Atmos. Ocean. Technol.* **2012**, *29*, 897–910. [[CrossRef](#)]
59. H Sparks, A.; Hengl, T.; Nelson, A. GSODR: Global Summary Daily Weather Data in R. *J. Open Source Softw.* **2017**, *2*, 177. [[CrossRef](#)]
60. Morabito, M.; Messeri, A.; Noti, P.; Casanueva, A.; Crisci, A.; Kotlarski, S.; Orlandini, S.; Schwierz, C.; Spirig, C.; Kingma, B.R.; et al. An Occupational Heat-Health Warning System for Europe: The HEAT-SHIELD Platform. *Int. J. Environ. Res. Public Health* **2019**, *16*, 2890. [[CrossRef](#)]

61. Alexander, L.V.; Zhang, X.; Peterson, T.C.; Caesar, J.; Gleason, B.; Klein Tank, A.M.G.; Haylock, M.; Collins, D.; Trewin, B.; Rahimzadeh, F.; et al. Global observed changes in daily climate extremes of temperature and precipitation. *J. Geophys. Res.* **2006**, *111*, D05109. [[CrossRef](#)]
62. Caesar, J.; Alexander, L.; Vose, R. Large-scale changes in observed daily maximum and minimum temperatures: Creation and analysis of a new gridded data set. *J. Geophys. Res.* **2006**, *111*, D05101. [[CrossRef](#)]
63. Wijngaard, J.B.; Klein Tank, A.M.G.; Können, G.P. Homogeneity of 20th century European daily temperature and precipitation series: Homogeneity of European Climate Series. *Int. J. Climatol.* **2003**, *23*, 679–692. [[CrossRef](#)]
64. Durre, I.; Menne, M.J.; Gleason, B.E.; Houston, T.G.; Vose, R.S. Comprehensive Automated Quality Assurance of Daily Surface Observations. *J. Appl. Meteorol. Climatol.* **2010**, *49*, 1615–1633. [[CrossRef](#)]
65. Josse, J.; Husson, F. MissMDA: A Package for Handling Missing Values in Multivariate Data Analysis. *J. Stat. Softw.* **2016**, *70*, 1–31. [[CrossRef](#)]
66. Tveito, O.E.; Aniskeviča, S.; Cappelen, J.; Engström, E.; Gjelten, H.M.; Jensen, C.D.; Jokinen, P.; Kuya, E.K.; Lussana, C.; Mäkelä, A.; et al. *ClimNorm—Temperature Data Set, Gap Filling Methods and Regional Analysis to Prepare New Climate Normals*; MET Report 04/2020; Norwegian Meteorological Institute: Oslo, Norway, 2020.
67. Muñoz-Sabater, J.; Dutra, E.; Agustí-Panareda, A.; Albergel, C.; Arduini, G.; Balsamo, G.; Boussetta, S.; Choulga, M.; Harrigan, S.; Hersbach, H.; et al. ERA5-Land: A state-of-the-art global reanalysis dataset for land applications. *Earth Syst. Sci. Data* **2021**, *13*, 4349–4383. [[CrossRef](#)]
68. Sheridan, S.C.; Lee, C.C.; Smith, E.T. A Comparison between Station Observations and Reanalysis Data in the Identification of Extreme Temperature Events. *Geophys. Res. Lett.* **2020**, *47*, e2020GL088120. [[CrossRef](#)]
69. Cerlini, P.B.; Silvestri, L.; Saraceni, M. Quality control and gap-filling methods applied to hourly temperature observations over central Italy. *Meteorol. Appl.* **2020**, *27*, e1913. [[CrossRef](#)]
70. Chervenkov, H.; Slavov, K. Geostatistical comparison of UERRA MESCAN-SURFEX daily temperatures against independent data sets. *IDŐJÁRÁS* **2021**, *125*, 123–136. [[CrossRef](#)]
71. Schulzweida, U. CDO User Guide. *MPI Meteorol.* **2022**. [[CrossRef](#)]
72. Pohlert, T. Trend: Non-Parametric Trend Tests and Change-Point Detection, R Package Version 0.0.1. 2015. Available online: [https://www.researchgate.net/publication/274014742\\_trend\\_Non-Parametric\\_Trend\\_Tests\\_and\\_Change-Point\\_Detection\\_R\\_package\\_version\\_001](https://www.researchgate.net/publication/274014742_trend_Non-Parametric_Trend_Tests_and_Change-Point_Detection_R_package_version_001) (accessed on 11 May 2022).
73. Vaidyanathan, A.; Kegler, S.R.; Saha, S.S.; Mulholland, J.A. A Statistical Framework to Evaluate Extreme Weather Definitions from a Health Perspective: A Demonstration Based on Extreme Heat Events. *Bull. Am. Meteorol. Soc.* **2016**, *97*, 1817–1830. [[CrossRef](#)]
74. Kendall, M.G. Rank Correlation Methods. *J. Inst. Actuar.* **1949**, *75*, 140–141. [[CrossRef](#)]
75. Sen, P.K. Estimates of the Regression Coefficient Based on Kendall’s Tau. *J. Am. Stat. Assoc.* **1968**, *63*, 1379–1389. [[CrossRef](#)]
76. Nairn, J.; Fawcett, R. The Excess Heat Factor: A Metric for Heatwave Intensity and Its Use in Classifying Heatwave Severity. *Int. J. Environ. Res. Public Health* **2014**, *12*, 227–253. [[CrossRef](#)]
77. R Core Team. *A Language and Environment for Statistical Computing*; Technical Report; R Foundation for Statistical Computing: Vienna, Austria, 2015.
78. RStudio Team. *RStudio: Integrated Development for R*; Technical Report; RStudio, Inc.: Boston, MA, USA, 2018.
79. QGIS Development Team. *QGIS Geographic Information System*; Technical Report; Open Source Geospatial Foundation Project: Beaverton, OR, USA, 2002.
80. Twardosz, R.; Walanus, A.; Guzik, I. Warming in Europe: Recent Trends in Annual and Seasonal temperatures. *Pure Appl. Geophys.* **2021**, *178*, 4021–4032. [[CrossRef](#)]
81. Jylhä, K.; Tuomenvirta, H.; Ruosteenoja, K.; Niemi-Hugaerts, H.; Keisu, K.; Karhu, J.A. Observed and Projected Future Shifts of Climatic Zones in Europe and Their Use to Visualize Climate Change Information. *Weather. Clim. Soc.* **2010**, *2*, 148–167. [[CrossRef](#)]
82. Oliveira, A.; Lopes, A.; Soares, A. Excess Heat Factor climatology, trends, and exposure across European Functional Urban Areas. *Weather. Clim. Extrem.* **2022**, *36*, 100455. [[CrossRef](#)]
83. Alexandrov, V.; Schneider, M.; Koleva, E.; Moisselin, J.M. Climate variability and change in Bulgaria during the 20th century. *Theor. Appl. Climatol.* **2004**, *79*, 133–149. [[CrossRef](#)]
84. Nairn, J.; Fawcett, R.; Ray, D. Defining and predicting excessive heat events: A national system. In Proceedings of the Extended Abstracts of the Third CAWCR Modelling Workshop, Melbourne, Australia, 30 November–2 December 2009; Volume 17.